

## STRESSING OF LOCKED PATCHES ALONG A CREEPING FAULT

BY SIMON T. TSE, RENATA DMOWSKA, AND JAMES R. RICE

### ABSTRACT

An analysis is presented of the stressing of locked patches along a fault zone which is creeping elsewhere. The model consists of strike-slip faulted elastic lithospheric plates loaded in a manner equivalent to imposition of a remotely uniform tectonic shear stress. The fault zone has an inhomogeneous strength distribution both depth-wise and along strike. It is modeled as being composed of locked patches and freely slipping parts treated as cracks. The solution is given with the use of the "line-spring" model which analyzes the problem by thickness-averaged plane stress theory for lithospheric plates which slip along a discontinuity cut at the plate boundary. As a boundary condition, thickness-averaged stress and slip at each local section along the cut was related to one another by the result of an antiplane strain analysis of slip for the crack or crack pair which describes the slipping and locked depth ranges at that section. The analysis indicates that the slip distribution along creeping parts of the fault, as well as the stress distribution along locked patches, depends strongly on the geometry of these zones. The model is used to examine stress concentrations associated with a slip-deficient seismic gap along strike and to study the effect of local irregularities in the margin of a locked region.

It is also used to simulate slip and stressing processes associated with the creeping portion of the San Andreas fault in central California, between the presently locked zones of the great 1906 and 1857 ruptures, and to constrain the nature of an apparently locked zone at the southeastern end which ruptures in characteristic Parkfield earthquakes. Near-fault creep and broadscale displacement data along the fault since the 1966 Parkfield earthquake and inferences from seismicity distributions are used. Limitations of the modeling procedure at short spatial wavelengths prohibit an accurate description of the Parkfield locked patch, but results suggest that it may be localized and occupy a small fraction of area of the normal seismogenic zone. An effective remote stressing rate of order  $0.3 \times 10^{-6} \times \text{shear modulus/yr}$  is inferred, together with a less well constrained 30 to 40 km lithospheric thickness, for consistency with the displacement data. Results enable estimates of stress accumulation along the locked 1857 rupture zone and the build-up of fracture energy release capability (of order  $10^7 \text{ J/m}^2$  in 150 yr) at its lower margin.

### INTRODUCTION

The accommodation of plate motion along a simple plate boundary occurs usually in a nonuniform fashion. At sufficiently great depths, because of temperatures and pressures prevailing there, motion is accommodated by aseismic shear or by predominantly aseismic shear together with small earthquakes. At shallower depths corresponding to the seismogenic zone, lithospheric rocks behave in a more brittle manner. During all but a few moments of the seismic cycle, they do not slide at all, or do so very little in the form of small earthquakes, so that stress accumulates and is released in the form of large earthquakes. The aseismic deformation below the shallower slip-deficient zone may be presumed to concentrate stress onto that zone, most notably along its lower margin. Thus, gradual rupture is promoted along the margin of the slip-deficient zone, especially during the latter part of the earthquake cycle when high stresses have accumulated, thereby enabling the slipping region to

penetrate into that zone and further concentrate stress onto it until loss of equilibrium occurs in the form of a large earthquake.

A portion of plate boundary may also be slip-deficient relative to other segments of comparable depth at neighboring locations along strike. Thus, neighboring earthquakes transmit stress along strike onto the less slipped zones. Such nonuniformity of slip along strike may be due to nonplanarity of the boundary as revealed by branches, bends, or en-echelon offsets of the fault trace, to irregularities along one of the plates (e.g., subducting seamounts), and to compositional variations. As a particular case, a shallow locked or slip-deficient region of plate boundary might be adjacent to another shallow region along strike which slips permanently (creeps) in a predominantly aseismic manner, thus leading to continuous stress concentration at the border of the locked zone.

We introduce here a simple quasi-static mechanical model which serves for analysis of some aspects of the stressing of locked patches along a strike-slip plate boundary during the earthquake cycle. In this way we are able to evaluate the effect of variations along strike of the geometry of such locked zones, and of the distributions of slip within them prior to locking (i.e., from previous earthquakes), on stress distributions over the locked regions and on deformations at the Earth's surface. Thus, the model provides a basis for linking seismicity distributions (stress-related) and geodetic observations to geometric characteristics of locked zones. We show a number of examples relating nonuniformity of locked-patch geometry and preslip to that of stress and surface deformation. Also, we apply the model to a part of the boundary between the North American and Pacific plates, namely the creeping portion of the San Andreas fault in Central California and the adjoining currently locked regions of the great 1857 and 1906 ruptures. Detailed modeling of the southern portion of the creeping region between Monarch Peak and Cholame is attempted in order to use geodetic and seismicity data to constrain the geometry of the locked zone which ruptures in characteristic Parkfield earthquakes, and thus to estimate stress accumulations there and in the adjacent region of the great 1857 rupture.

Our modeling is performed in a simple manner using a variant of the "line spring" procedure (Dmowska and Li, 1982; Li and Rice, 1983a, b). In the present work, we assume that during the time periods considered constant resistive shear stresses act on the base of the lithosphere near the plate margin and along slipping zones at the plate boundary. Hence, periods of active coupling to viscoelastic processes in the asthenosphere and to time-dependent down-dip slip resistance at the plate boundary are excluded. Such coupling is important in the postseismic period of rapid-redistribution of coseismic stress changes through such relaxation processes, and possibly also in a shorter time precursory period before a great earthquake [e.g., Li and Rice (1983a, b) explain that the comparatively rapid preinstability advance of slip into the locked zone would be resisted partly by short-time elastic response in the asthenosphere]. Here, we neglect changes in size of the locked regions due to advance of the slipping zones into them, although such advance is considered explicitly in the references cited and also in work by Stuart (1979a, b) and Stuart and Mavko (1979). Also, work based on the line spring procedure is more accurate the more gradually the geometry of locked zones varies along strike. This inability to resolve accurately at short spatial wavelengths along strike ultimately limits an accurate description by our procedure of the locked patch near Parkfield.

Many investigators (Wesson *et al.*, 1973; Bakun *et al.*, 1980; Lay and Kanamori,

1981; Lindh and Boore, 1981; Dmowska and Li, 1982) have used this concept of locked patches to explain spatial and temporal variations of seismicity and slip rate along a plate boundary. Based on study along the central San Andreas fault, Wesson *et al.* (1973) related seismically active areas with regions of steep gradients or low values of surface fault-slip rate. Bakun *et al.* (1980) used rupture propagation directivity of precursory shocks and aftershock distributions to infer stuck patches along the Cienega Road section of the San Andreas fault. Relating the foreshocks and point of initiation of the main shock of the 1966 Parkfield earthquake to the

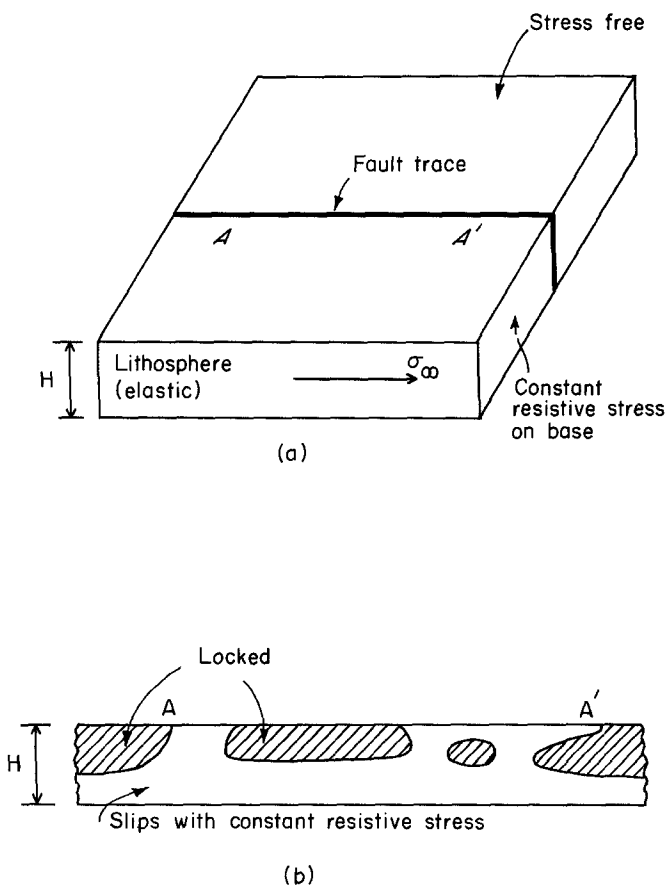


FIG. 1. (a) Elastic lithospheric plate containing boundary of strike-slip type. (b) Plate boundary consists of locked and slipping zones.

geometric bend of the trace at the Parkfield region, and relating the en-echelon offset near the Cholame area to the stopping of the rupture, Lindh and Boore (1981) suggested a locked patch of  $5 \times 25$  km centered on the 1966 aftershock zone. The above line of work implies that locked patch geometry is closely related to the slip rate distribution and seismicity pattern along a fault, but so far there are no direct attempts to link them together.

#### MECHANICAL MODEL OF A STRIKE-SLIP FAULT

The mechanical model as shown in Figure 1a considers the lithosphere as a linearly elastic isotropic plate of uniform thickness  $H$  containing a planar vertical

boundary of strike-slip type. The plate is subjected to remote loadings which would transmit a uniform shear force  $\sigma_\infty H$  across the plate boundary per unit distance along strike, at least if the fault slip did not vary along strike. The top of the plate (Earth's surface) is free of shear stress, and we consider situations for which effectively constant resistive shear stresses act on the base of the plate at its contact with the asthenosphere, at least near the plate boundary, and also along all sliding portions of the vertical boundary. Hence, if we regard  $\sigma_\infty$  as the loading which accumulates during some time period for which these resistive stresses are constant, we may analyze the stressing problem as that for a plate which is stress free at top and bottom and along sliding portions of the vertical boundary.

Figure 1b shows the longitudinal cross-section of the plate boundary (AA') which is assumed to consist of slipping and locked zones. In different circumstances, the boundary may have the form of: (i) an effectively locked shallow seismic gap zone of the first kind extending a long distance along strike; (ii) one or a few smaller nonslipping asperities within slipping or recently slipped surroundings on a fault plane; or (iii) a transition zone from a long-term creep slipping to a locked segment along strike. The San Juan Bautista and Parkfield ends of the creeping segment of the San Andreas fault are examples of the latter kind. The origin of the asperities or patches is generally thought to be due to geometric complexity and material inhomogeneity as mentioned previously. The locked patches are assumed to be fixed in position during the time period considered. Both elastic-brittle crack modeling by Li and Rice (1983a, b) and frictional slip modeling by Mavko (1984) and Tse and Rice (1984) suggest that this is an acceptable first approximation, in that during much of the earthquake cycle the boundary between the slipping and effectively locked regions changes little in position.

As a whole, from an elastic-brittle crack mechanics point of view, the fault zone is regarded as a part-cracked section with variable crack depth and geometry in an infinite plate subjected to uniform remote shear stress loading  $\sigma_\infty$ . In general, this three-dimensional crack problem is not easily solved, but with the use of the line-spring procedure introduced by Rice and Levy (1972), an approximate solution becomes tractable. The line-spring model was introduced for the analysis of part-through surface cracks in tension-loaded elastic plates or shells [see, Parks *et al.* (1981), Parks (1981), and Delale and Ergodan (1982) for recent applications in that context]. Li and Rice (1983a, b) have applied the model to strike-slip ruptures in tectonic plates.

The idea of the line-spring procedure is to reduce the complicated three-dimensional crack problem (Figure 1a) into two simple two-dimensional plane problems. The thickness averages of the stresses and displacements in the lithosphere will satisfy approximately elastic plane stress theory. Within this theory, the lithosphere may be represented as a two-dimensional plane, the  $x$ - $y$  plane as shown in Figure 2a, and there is a line of (mode II) slip discontinuity along the  $x$  axis representing the fault trace. Recognizing that this model is linear and using dislocation theory, the thickness averaged shear stress  $\sigma(x)$  is related to the thickness averaged slip  $\delta(x)$  along  $y = 0$  by (e.g., Li and Rice, 1983a)

$$\sigma(x) = \sigma_\infty - \frac{(1 + \nu)}{2\pi} \mu \int_{-\infty}^{\infty} \frac{1}{x - x'} \frac{\partial \delta(x')}{\partial x'} dx' \quad (1)$$

where  $\mu$  and  $\nu$  are the shear modulus and Poisson's ratio, respectively. The integral term of equation (1) is the thickness-averaged stress response due to the presence

of a dislocation (slip gradient) distribution along some portion the  $x$  axis. On the other hand, the thickness-averaged slip  $\delta(x)$  at the plate boundary can be regarded as a function of the thickness averaged stress  $\sigma(x)$  there. As suggested by Figure 2b, it is assumed within the model that the local thickness-averaged slip and stress at a section at position  $x$  along strike are related to one another just as would be

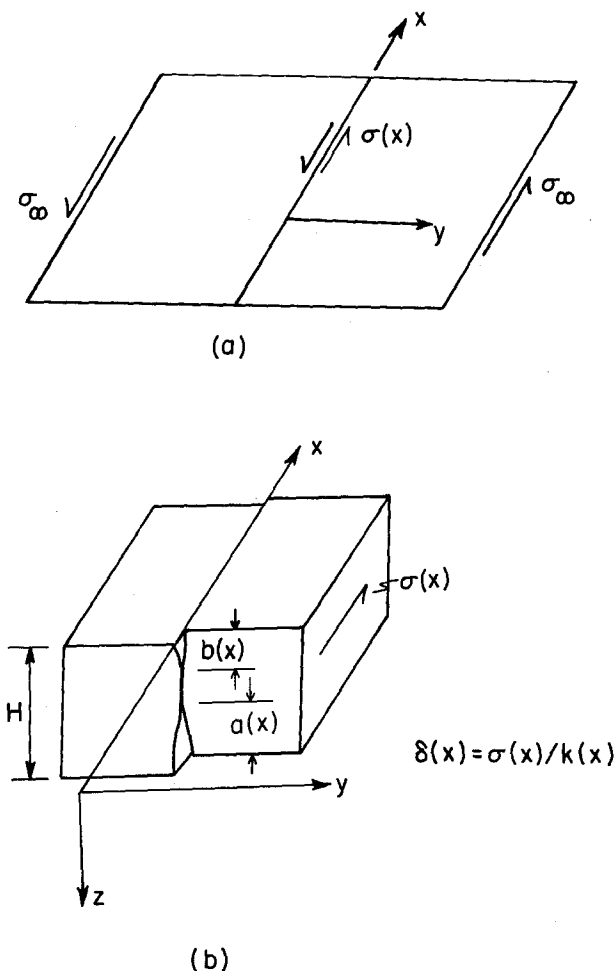


FIG. 2. Line-spring procedure. (a) Stress transmission in lithospheric plate is modeled by two-dimensional plane stress for thickness averages of stress  $\sigma$  and slip  $\delta$ . (b) Local relation between  $\sigma$  and  $\delta$  at given section  $x$  along strike in (a) obtained by two-dimensional antiplane shear analysis for depth-wise configuration of slipping and locked zones at that section. Antiplane analysis is presented in the Appendix.

predicted by a two-dimensional antiplane strain analysis of mode III slip, based on a depth variation of locked regions appropriate to the section at position  $x$ .

When all portions of boundary are regarded as being either completely locked or freely slipping, as in the present work, this relation is  $\sigma(x) = k(x)\delta(x)$ , where  $k(x)$  is a proportionality constant (the line-spring stiffness). It depends on the fault zone geometry at  $x$ , and we derive its value in the Appendix, equation (A14), by solving the mode III crack problem depicted in Figure 2b

$$k(x) = \left( \frac{\pi\mu}{2H} \right) / \ln \left\{ 2 / \left[ \cos \frac{\pi a(x)}{H} + \cos \frac{\pi b(x)}{H} \right] \right\}. \quad (2)$$

Here,  $a(x)$  and  $b(x)$  are crack depths at  $x$  such that the locked patch extends from  $z = b$  to  $z = H - a$ . Therefore, equations (1) and (2) constitute a full formulation for the thickness-averaged stress and slip for a general fault zone geometry. Once  $\sigma(x)$  is determined by solution, quantities like local shear stress  $\tau_{xy}$  within the locked patches, surface slip and surface strain near the fault trace, and crack tip stress intensities and energy release rates can be found immediately. Formulas are given in the Appendix and involve the unknown  $\sigma(x)$  times known functions of  $a(x)$ ,  $b(x)$ , and depth  $z$  or distance  $y$  from the fault trace, as appropriate.

For numerical solution, the indefinite integral term in equation (1) can be reduced to a definite integral over a finite interval as follows. It will generally be appropriate to assume that at great distances, denoted by  $|x| > L$ , from the fault zone considered, the plate boundary is locked from the Earth's surface to a certain uniform depth,  $H - a_\infty$ , and if  $L$  is chosen large enough, the thickness-averaged stress will be effectively constant at  $\sigma_\infty$  and the thickness average slip effectively constant at  $\delta_\infty = \sigma_\infty/k_\infty$  at distances for which  $|x| > L$ . Here,  $k_\infty$  is calculated from equation (2) with  $b = 0$ ,  $a = a_\infty$ . Hence, the indefinite integral term in equation (1) can be rewritten as

$$\frac{\mu(1+\nu)}{2\pi} \int_{-\infty}^{\infty} \frac{1}{x-x'} \frac{\partial \delta(x')}{\partial x'} dx' = \frac{\mu(1+\nu)}{2\pi} \left\{ \frac{\delta_\infty}{x-L} - \frac{\delta_\infty}{x+L} + \int_{-L}^L \frac{1}{x-x'} \frac{\partial \delta(x')}{\partial x'} dx' \right\}. \quad (3)$$

Equivalently, the first and second terms on the right-hand side of equation (3) can be interpreted as the stress responses at  $x$  due to dislocations in thickness-averaged slip of magnitude  $\delta_\infty$  at  $+L$  and  $-L$ , respectively. Combining equations (1), (2), and (3) gives

$$k(x)\delta(x) + \frac{\mu(1+\nu)}{2\pi} \int_{-L}^L \frac{1}{x-x'} \frac{\partial \delta(x')}{\partial x'} dx' = \sigma_\infty \left[ 1 + \frac{\mu(1+\nu)}{\pi k_\infty} \left( \frac{L}{L^2 - x^2} \right) \right]. \quad (4)$$

Once remote stress  $\sigma_\infty$  and a particular distribution of locked and slipping zones are specified [i.e.,  $a(x)$  and  $b(x)$  are given so that  $k(x)$  can be determined], the thickness-averaged slip  $\delta(x)$  is readily solved from equation (4). The integral term in equation (4) is approximated by the following discretization: the length  $2L$  is divided into  $n$  (200 to 300) intervals of equal length, in each of which  $\delta$  is given some unknown but uniform value, and we require that the equation be satisfied exactly for the  $x$  values at the mid-points of the intervals. This procedure reduces equations (4) into a set of  $n$  linear equations with  $n$  unknown  $\delta$ 's, solved by standard procedures.

The line-spring model as formulated is plainly more accurate in representing the actual three-dimensional situation the more gradually the crack depths  $a(x)$  and  $b(x)$  change with distance  $x$  along strike. For accuracy, one would prefer that parameters like  $(H/a)da/dx$  or  $H/\bar{L}$ , where  $\bar{L}$  is a characteristic scale length along strike, be small compared to unity. Nevertheless, comparisons of model predictions of stress intensity factors for semi-elliptical surface cracks in tension-loaded plates, in the references cited above, with three-dimensional numerical elastic solutions suggest that the model remains quite accurate even when the above condition is widely violated, e.g., when the surface length of the crack is of order of plate

thickness. This provides encouragement in applying the model to some of the cases presented here, although a particular application of the model to be discussed for the Parkfield area is limited by this inadequacy at short spatial wavelengths along strike.

In some cases, we are concerned with locked regions which have a nonuniform distribution of previous slip along strike. For example, suppose that at section  $x$  along strike the presently locked portion of plate boundary between  $z = b(x)$  and  $H - a(x)$  has average slip  $D(x)$ . Then for the thickness-averaged slip  $\delta$ , we would have  $\delta = D(x)$  if that section of boundary were cut free from the surrounding plates. However, the actual interaction with these plates results in transmission of a thickness-averaged stress  $\sigma(x)$  at  $x$ , and therefore we have to use  $\delta(x) = D(x) + \sigma(x)/k(x)$  for the thickness-averaged slip at  $x$ . When this expression is used to replace  $\sigma(x)$  in equation (1), we obtain an identical integral equation to that described earlier, except that the forcing term  $\sigma_\infty$  is replaced by  $\sigma_\infty + k(x)D(x)$ . The indefinite integral is reduced to one over a finite interval for numerical solution by a procedure analogous to that described earlier, but using  $\delta_\infty = D_\infty + \sigma_\infty/k_\infty$  for  $|x| > L$ . Here  $D_\infty$  is the value of  $D(x)$ , assumed constant, at great distances from the region of interest.

### STRESSING OF LOCKED PATCHES

We show some representative results here. First consider a boundary (Figure 3) which is locked over the upper third of the plate thickness and slipping below, but with small nonuniformities of the locked zone margin. In the case shown, these have the form of bell-shaped Gaussian variations of  $a(x)$  from its average value  $2H/3$ . The maximum amplitude of the disturbances is one-third the locked zone thickness (i.e.,  $H/9$ ), and the width  $2s$  of the bell shapes along strike is  $H/4$ , where  $s$  is the variance of the Gaussian. Here, there is no nonuniformity of preslip ( $D = 0$ ), and loading is by a uniform thickness-averaged stress  $\sigma_\infty$ .

Figure 3 shows the result for  $\delta(x)$  obtained by numerical solution and from it one computes the thickness-averaged stress  $\sigma(x) = k(x)\delta(x)$ . Both of these mirror the original nonuniformity, the stress more markedly so. Note that the average stress over the locked zone depth is  $\sigma H/(H - a)$  and is less sharply peaked than is  $\sigma$ . The actual local distribution of stress  $\tau_{xy}$  within the locked zone could be computed in terms of  $\sigma(x)$  and  $a(x)$  from equation (A15). It is strongly concentrated toward the margin of the locked zone, which is a crack tip (Figure 2b). A measure of the crack tip stress concentration is provided by the energy  $G$  that would flow to the crack tip per unit area of advance of the slipping region into the locked region [see, equation (A21)], and the procedure for calculating  $G$  is explained in the Appendix. Results obtained from the distributions of  $\sigma(x)$  and  $a(x)$  by use of equations (A16) and (A18) or, equivalently, equation (A23) are shown in Figure 3.  $G$  is largest where the deep locking at the center of the figure has impeded slip and concentrated stress. It is smallest at the locations of shallow locking, which provide compliant portions of plate boundary and shield themselves from stress. Nevertheless, it is interesting that  $G$  and, less strikingly,  $\sigma$  show modest peaks to the sides of the regions of shallow locking (analogous valleys occur to the sides of the deep locking). If we regard the shallow locking as the result of moderate earthquakes, which have converted a previously locked zone into a slipping zone, then the adjoining peaks in  $G$  suggest a tendency for further seismicity to occur preferentially at adjacent locations.

As a second example, we consider in Figure 4 more drastic perturbations of the locked zone. We may interpret what is shown there as a simple model for a stretch of plate boundary where regions of two comparatively recent great earthquakes surround an area which has not slipped for a long time, i.e., a seismic gap of the first kind. In the present discussion, we treat the regions of recent earthquakes as

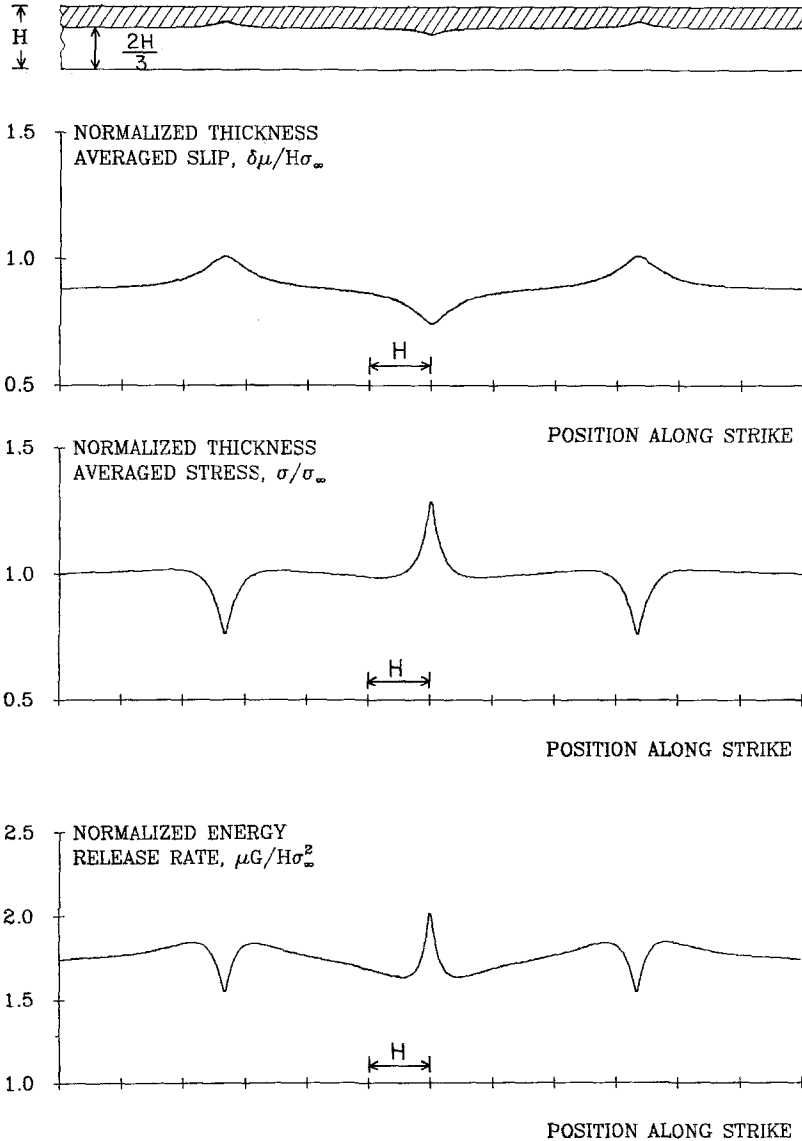


FIG. 3. Effects of local nonuniformities in depth of a locked zone over upper third of plate thickness; free slip is below. Loading is by thickness-averaged remote stress  $\sigma_\infty$ . See text for details.

completely destressed although, because of healing processes, they probably are able to carry some stress a short time later. We consider the area of the seismic gap as a slip-deficient, completely locked region although minor small seismicity in this area might allow some accommodation of plate motions, i.e., some slip. Also, we assume that below the locked zone, the motion between the two plates is accommodated by stable, free sliding. The resulting solution for  $\delta$  is shown for uniform remote thickness-averaged stressing by  $\sigma_\infty$ .

The thickness-averaged stress distribution in the region of the seismic gap and variation of energy release rate along the lower edge of the locked patch are also shown in Figure 4 [from equations (A24) and (A25) the average value of  $G$  along the vertical edges of the locked path is 0.44 of the peak values shown, or about 1.2

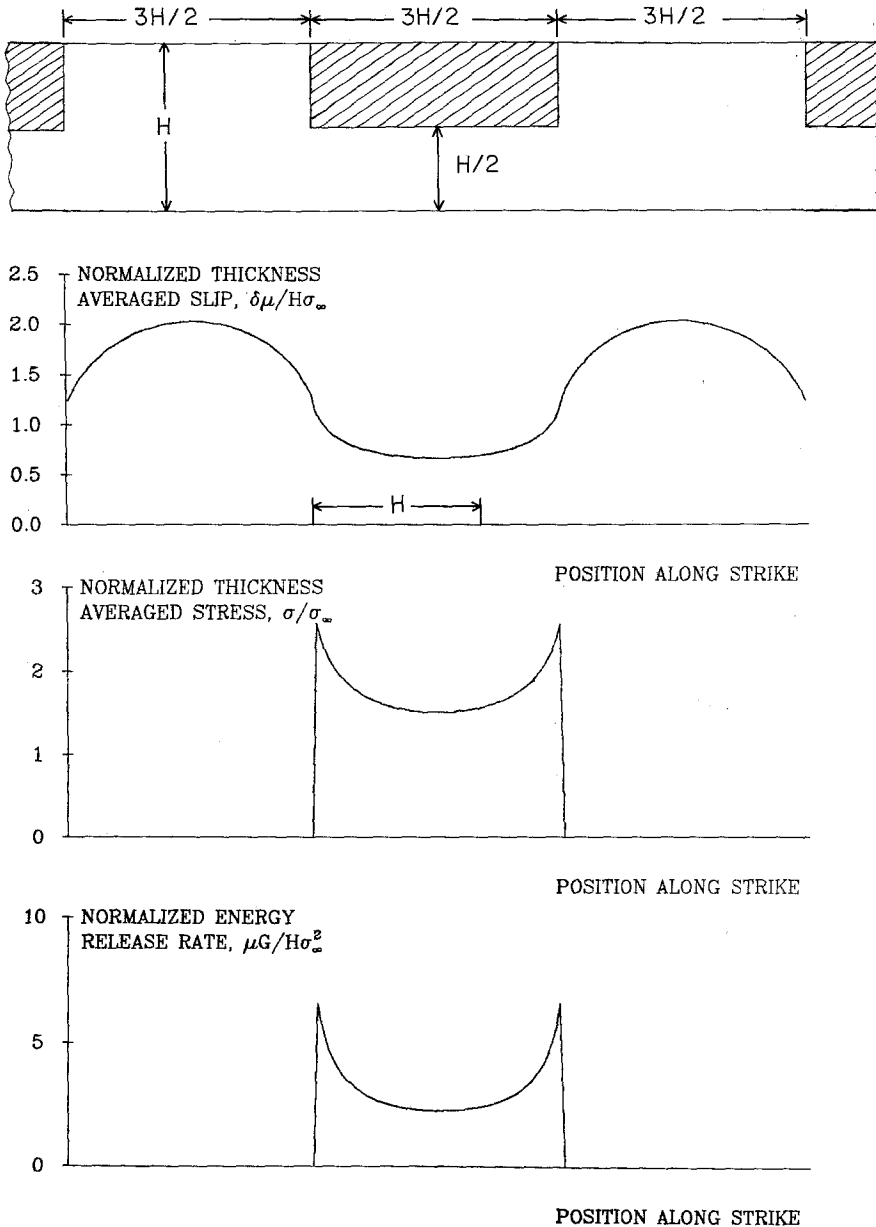


FIG. 4. Simulation of seismic gap by freely slipping zones to the sides of (and below) a locked patch, with loading by thickness-averaged remote stress  $\sigma_\infty$ .

times the minimum value at the center of the patch]. High stress concentrations exist at the ends of the slip-deficient patch, and the stresses diminish toward the center of that region.

Relaxing a little our assumptions that areas on both sides of a locked patch (i.e., areas of recent great earthquakes along the plate boundary) carry no stress and

allowing them to carry some stress, and also allowing some slip in the area of the locked patch itself, would not change qualitatively our results which show the highest stresses at both ends of the locked zone and, also, additional stress concentrations associated with complexities of asperity structure (Figure 3). Following the model of Dmowska and Li (1982), for such seismic gaps, we interpret these regions of higher stresses as areas responsible for higher seismicity, as often observed in seismicity gaps of the first kind along plate boundaries (see, e.g., Kelleher *et al.*, 1973; Kelleher and Savino, 1975; Mogi, 1979). Regions of higher stress are also sites of nucleation of great ruptures (Dmowska and Li, 1982). In most cases of great earthquakes, the rupture starts near one end of the gap zone and runs toward the other (see, e.g., Kelleher and Savino, 1975); exceptionally, it starts somewhere in the gap area and develops bilaterally. In the light of our modeling, the latter behavior might be caused by more complex asperity structure (e.g., two or more asperities close to each other).

Figure 5 shows another approach within our modeling procedure for analyzing a seismic gap of the first kind. As in a discussion of the Dmowska and Li model by Rice (1983), we assume that the effect of neighboring earthquakes is to slip and relock the shallow seismogenic zone, and that after relatively short-time postseismic adjustments, a stable freely slipping response continues below. This is a case of nonuniform pre-slip of the locked zone as discussed at the end of the previous section. Three distributions for the preslip dislocation  $D(x)$  are shown. Case (a) has an abrupt change from zero to  $D_{\max}$ , whereas cases (b) and (c) have exponential approach, with respective  $1/e$  decay lengths of  $H/5$  and  $H/2$ , to  $D_{\max}$ . Here, the slip-deficient gap zone has length  $3H$ . We show only the right half of all figures, which are symmetric about the center line. Also, we neglect the effect of remote stress  $\sigma_{\infty}$  and show only the effect of the nonuniform preslip.

The results for thickness-averaged slip  $\delta$  in Figure 5 are seen to be smoother versions of the preslip  $D$ . Also, the adjacent preslip induces some thickness-averaged slip along the gap zone, due to slip that has been induced below the completely locked patch. The resulting stresses are also shown, and their distribution is consistent with the tendencies for higher seismicity and rupture nucleation at the ends of a gap as discussed earlier.

#### MODEL OF CREEPING SECTION OF SAN ANDREAS FAULT NEAR PARKFIELD

In this section, we use our procedures to suggest possible geometries and stress distributions for locked regions along and adjacent to the creeping section of the San Andreas fault in central California (Figure 6). We are interested here particularly in the configuration (and stress distribution) of such patches during most of the cycle of Parkfield characteristic earthquakes. We omit the part of the cycle which follows the earthquakes and is characterized by afterslip effects associated with comparatively rapid stress redistribution after the earthquake, and, also, we omit the last part of the cycle, preceding the earthquake, possibly characterized by accelerating slip and leading to the earthquake itself. To deal with these phases we would, according to the estimates of Li and Rice (1983b), have to include coupling to the asthenosphere and to examine the advance of slip zones into locked patches, and perhaps also revise the assumption of slip at constant resistive stress. Parkfield earthquakes recur with the interval of about 21 yr for the last 6 events (Bakun and McEvelly, 1984; Stuart *et al.*, 1985), apart from the one decade earlier 1934 event, so we are studying here perhaps the middle 16- to 18-yr period of a representative cycle. We also assume in our calculations that there is an approximately constant

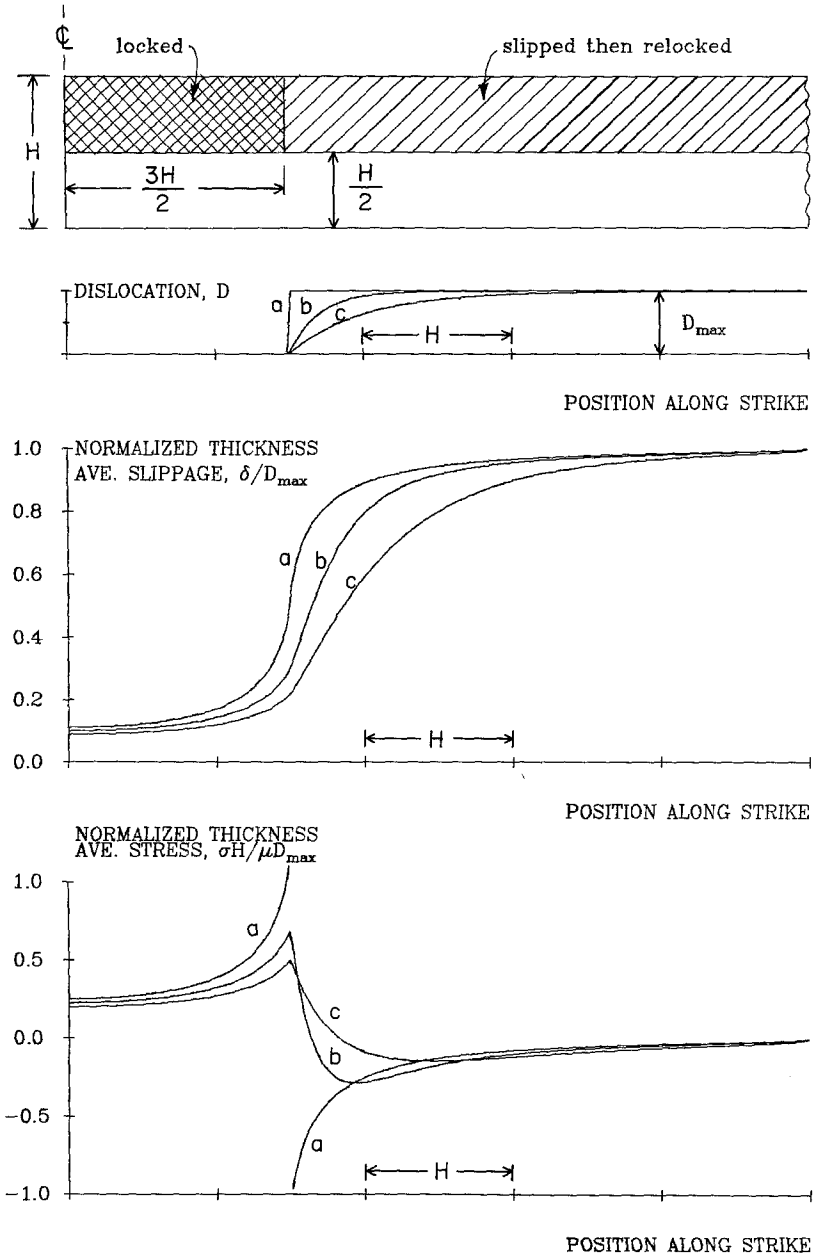


FIG. 5. Simulation of seismic gap by a locked shallow zone bordered on sides by shallow zones that were preslipped by dislocation  $D$  and then relocked. Free slip is below locked zones. Right half of the configuration is shown with coordinate origin at the center line.

distribution in space and time of locked patches along the fault for the period of our slip and stress simulation, although seismicity near Parkfield shows a tendency for migration which we will discuss further. To assess this distribution, we take into account the surface slip distribution as measured along the fault since the last (1966) Parkfield earthquake, as well as seismicity patterns in this area, and source studies of the 1966 Parkfield earthquake.

Figure 7 shows the long-term slip rate distribution along the fault between 1966 and 1980 taken from near fault (10 to 100 m), intermediate-scale (1 to 2 km) and

broad-scale (10 km and over) measurements. The near-fault measurements include data from Burford and Harsh (1980) based on alignment arrays from 1966 to 1978 and data from Schulz *et al.* (1982) based on creepmeters from 1968 to 1980. The intermediate-scale measurements are reported by Lisowski and Prescott (1981) based on a short-range network from 1975 to 1979. Lisowski and Prescott also report the broad-scale measurements based on a Geodolite network and assuming simple block motion from 1969 to 1978. The range along strike and error intervals are indicated for the broad-scale measurements. The near-fault and intermediate-scale measurements are in close agreement except at Monarch Peak where the latter is considerably higher than that inferred from near fault measurement. This

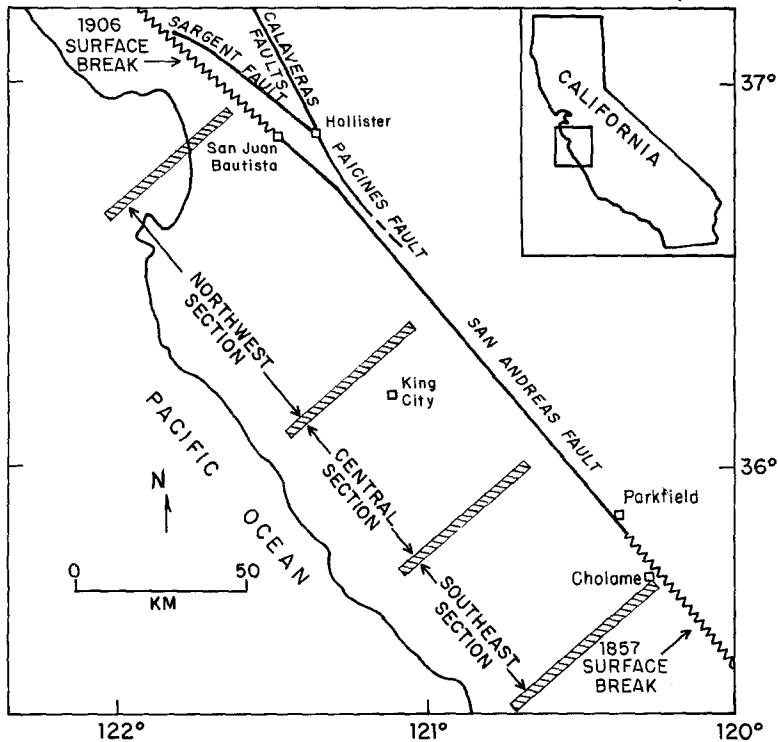


FIG. 6. Creeping section of the San Andreas fault (after Burford and Harsh, 1980).

indicates that the zone of active deformation is confined to a narrow width of less than 200 m (Burford and Harsh, 1980; Lisowski and Prescott, 1981). Rymer *et al.* (1984) point out that the excess of slip rate recorded by the short range (intermediate-scale) network over near-fault measurement at Monarch Peak is due to the additional contribution from the subsidiary faults in the region. The measured slip rate increases with the perpendicular distance from the fault trace, i.e., the near-fault measurements are the lowest, and the broad-scale measurements are the highest. Within the mechanical model proposed in this paper, this trend of increase of surface slip rate with distance away from fault trace can be seen from equation (A11). There are large discrepancies in slip rates between broad-scale and near-fault measurements in the northwestern end of the creeping section. Lisowski and Prescott (1981) explain that the broad-scale geodolite network which covered a 20-km-wide deformation zone could pick up additional displacement due to the nearby

Calaveras fault. There seems also to be a trend of moderately larger broadscale measurements near Parkfield where the array measures over approximately a 10 km distance measured perpendicular to the fault. This provides a constraint on the ratio of displacement rates at  $\pm 5$  km from the fault to those at the fault trace. The ratio would be approximately unity (except near the ends of the creeping zone), for example, if the creeping section penetrated through the entire lithospheric thickness without locked patches.

Following Burford and Harsh (1980), Figure 6, the 180-km-long creeping section of the San Andreas fault may be divided into three subsections: (1) a 80-km-long northwestern section from San Juan Bautista to Bitterwater; (2) a 55-km-long central section from Bitterwater to Slack Canyon; and (3) a 45-km-long southeast section from Slack Canyon to a few kilometers southeast of Cholame. Both Burford

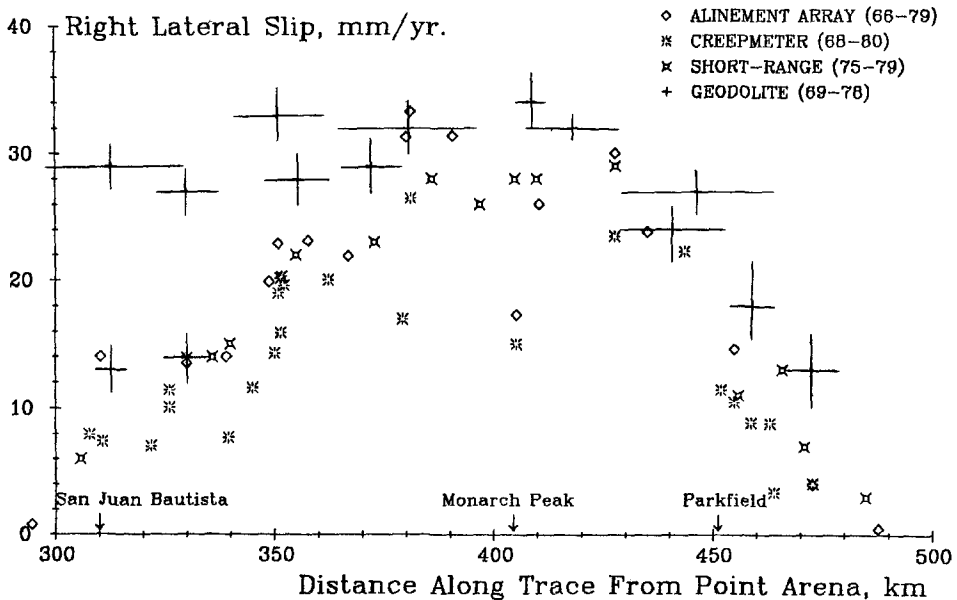


FIG. 7. Slip rate along the San Andreas fault from 1966 to 1980. See text and references for further discussion.

and Harsh (1980) and Schulz *et al.* (1982) report that steady-state creeping is observed in the central section except for the area around Monarch Peak which shows occasional small shocks. The two sections flanking the central section are characterized by regional decreases in creep rates outward toward the limits of surface ruptures associated with the great 1857 and 1906 earthquakes. These two sections also show relatively high levels of minor seismicity and occasional moderate earthquakes while the regions corresponding to great rupture have shown neither creep nor seismic activity since the last ruptures. It is also pointed out by Wesson *et al.* (1973) that areas of steep gradients or relatively low values of creep rate are usually underlain by patches characterized by relatively high seismicity. Hence, there seems to be a general presumption that the central section can be regarded as a freely slipping zone while the two flanking sections are slipping-to-locked transition zones with local locked patches that rupture in moderate earthquakes. The positions and depth of these patches are further constrained by seismicity patterns along the fault.

Figure 8 from Wesson *et al.* (1977) and Burford and Harsh (1980) shows the epicenters of minor earthquakes during the period 1969 to 1976. It is seen that the seismically active areas correspond closely to the areas of steep gradient of creep rate or relatively low creep rate as mentioned above. The depths of earthquakes are

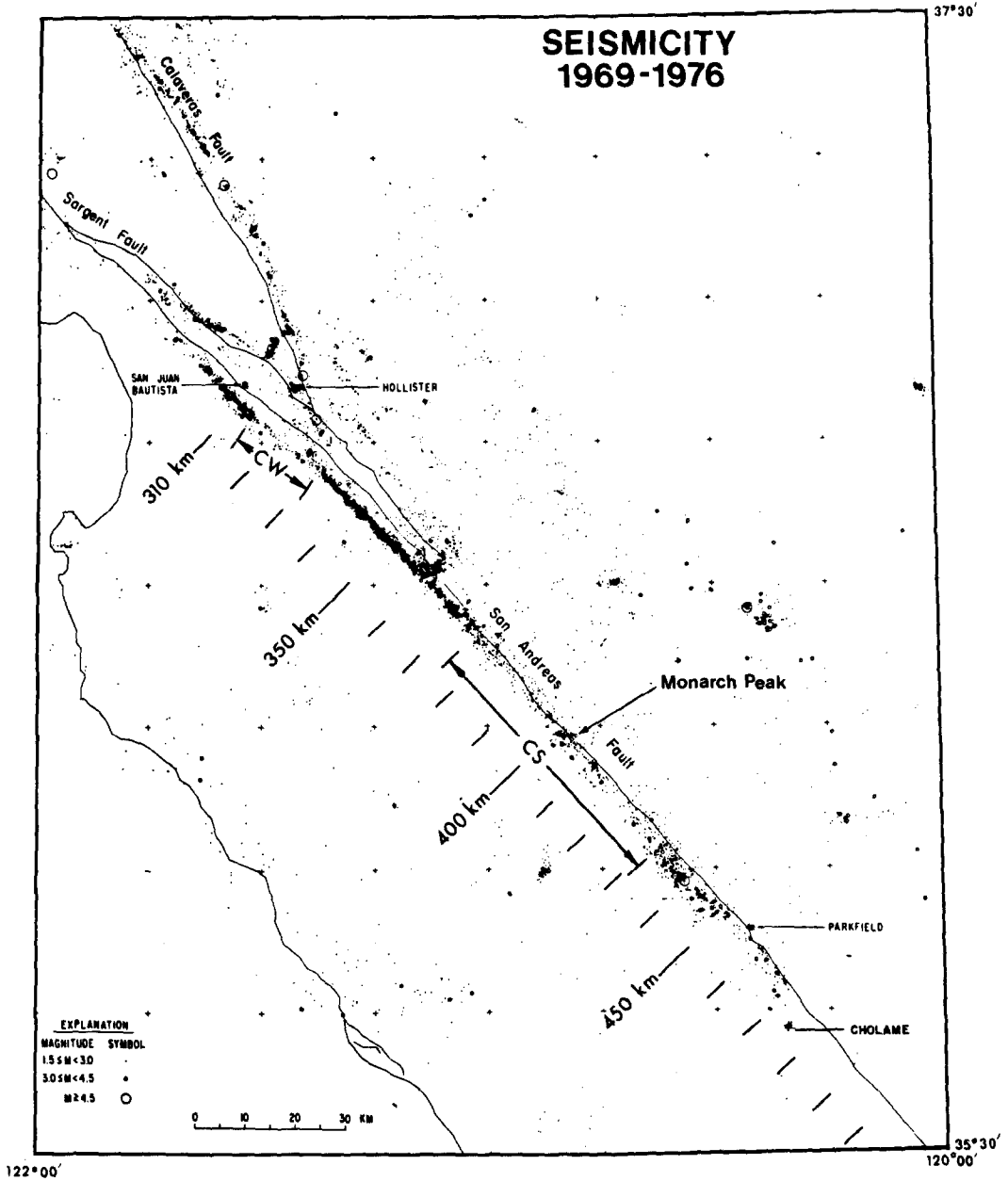


FIG. 8. Seismicity (1969 to 1976) along a portion of the San Andreas fault shown previously (after Wesson *et al.*, 1977; Burford and Harsh, 1980).

concentrated between 3 and 12 km. No earthquakes below 15 km are found (Eaton *et al.*, 1970; Wesson *et al.*, 1973). For simplicity and with the notion that the detail of the patch geometry at one end does not affect very much that at the other end, the San Andreas fault is taken to be symmetric about Monarch Peak, and we concentrate only on the patch geometries in the Parkfield-Cholame section.

Figure 9 from Kerr (1984), who credits A. Lindh as its source, shows seismicity distributions near the 1966 Parkfield focus in different time intervals. If it is reasonable to regard such seismicity as a sign of stress concentrations near the border of the locked zone as we have discussed earlier, and if that same kind of stress concentration led to the 1966 foreshock and main shock, then we would have to regard the locked region as extending to depths of order to 10 to 12 km, at least near Parkfield. This is further supported by results of O'Neill (1984) who shows that earthquakes of moderate stress drop occur in that depth range, and by the limit at around 10 km to aftershocks of the 1966 event (Figure 9).

The situation is as follows: since there are earthquakes which nucleate in the vicinity of Parkfield and propagate to the southeast, and since the area is seismically active (Figure 8), we assume that there is a locked patch near Parkfield extending at least somewhat to the southeast. Since surface creep is observed along the fault

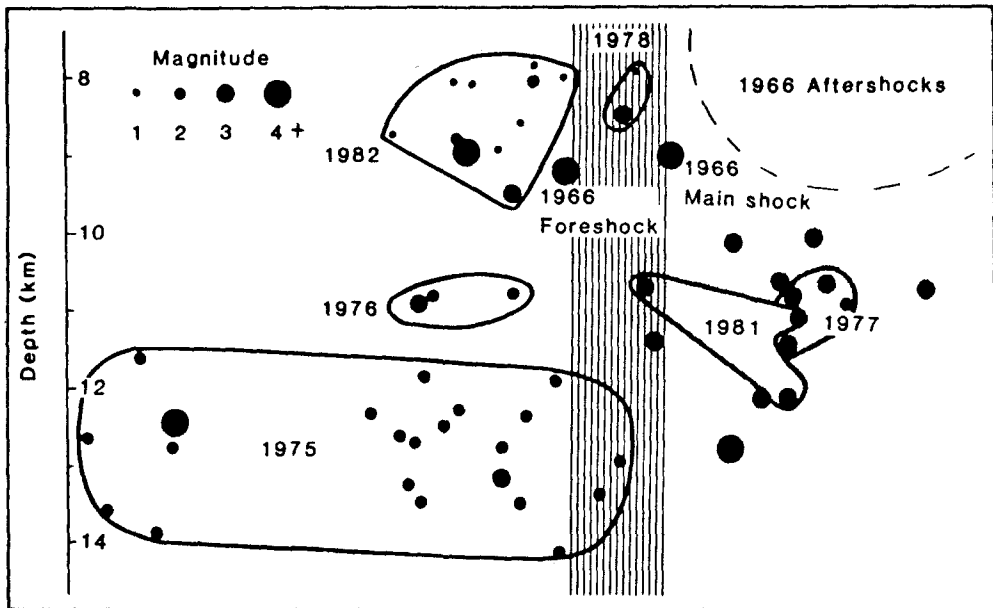


FIG. 9. Seismicity during recent time periods near Parkfield, in the vicinity of the nucleation site for the 1966 main shock (after Kerr, 1984; based on A. Lindh as source).

trace around Parkfield and to the southeast toward Cholame, we observe that this patch cannot extend to the surface there, but must extend to the surface to the south along the main part of the 1857 rupture where there is no measured creep. The northwestern end of the inferred patch corresponds roughly to the 5° bend of the fault trace near Parkfield (Segall and Pollard, 1980; Lindh and Boore, 1981). The limit to its southeastern end is at the right-stepping offset near Cholame. In order to further constrain the patch geometry, as well as the appropriate lithospheric thickness  $H$  and remote stress rate  $\dot{\sigma}_{\infty}$  for the region, we wish to fit the measured slip rate along the fault trace taking cognizance also of: (1) broadscale geodetic measurements at the fault trace near Parkfield, as in Figure 7 and (2) depths of seismicity, as in Figure 9. Unfortunately, we find that items (1) and (2) lead to rather different fits when applied to the geometry of locked zones shown in Figures 10 to 12, and we are reluctant to attempt further refinement of the geometrical structure of the locked zone along strike owing to inadequacies of our calculation procedure, especially for surface slip, at short spatial wavelengths along strike.

We first present the results which are responsive either to item (2) or (1) above and then discuss their interpretation more fully at the end of this section. In all cases shown, we have used a model (Figures 10 to 12) which is symmetric about Monarch Peak, has a freely slipping zone over the entire plate thickness for 35 km

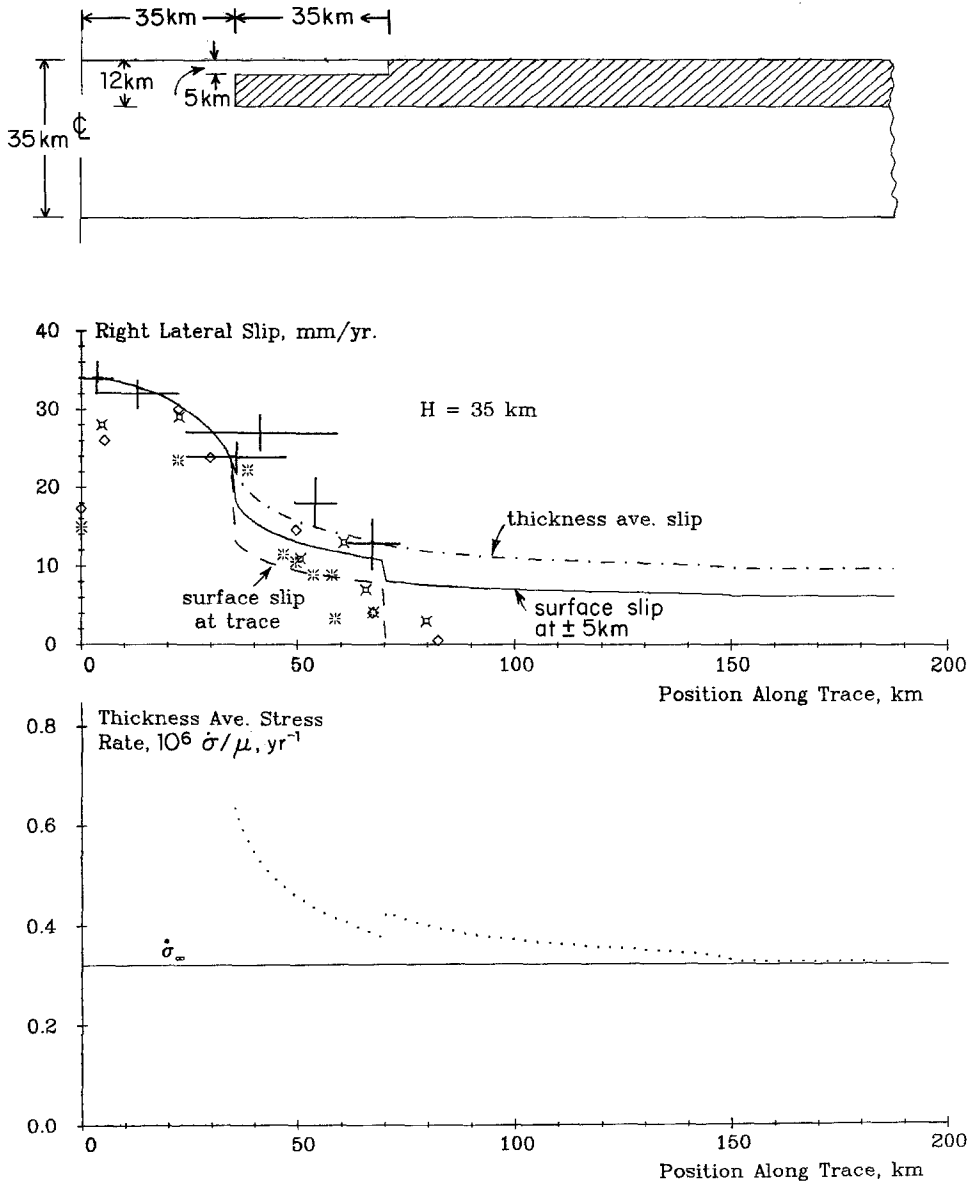


FIG. 10. A fit-to-creep data at the fault trace with the lower margin of the locked region chosen from depth of the seismicity considerations. Note that the broadscale slip rate data near Parkfield (i.e., displacements at  $\pm 5$  km) are underpredicted. Resulting stress rates and inferred  $\dot{\sigma}_\infty$  are also shown.

southeast along the fault trace from Monarch Peak, has a submerged locked patch of parameters  $b$ ,  $a_p$  beginning near the 1966 Parkfield epicenter and extending over the next 35 km southeast (i.e., from about 12 km northwest to 23 km southeast of Parkfield), and has a locked patch with  $b = 0$  and  $a = a_\infty$  further to the southeast along the 1857 break.

In Figure 10 we have chosen  $H - a_p = H - a_\infty = 12$  km from depth of seismicity considerations, item (2) above, and find  $b = 5$  km,  $H = 35$  km, and  $\dot{\sigma}_\infty/\mu = 0.32 \times 10^{-6}/\text{yr}$  give reasonable fits for all but the broadscale measurements near Parkfield. Recall that the near-fault data at the origin, i.e., in the vicinity of Monarch Peak, should be disregarded for the reason noted earlier. The slip and stress rate curves scale directly with remote stress rate, and the value quoted corresponds to  $\dot{\sigma}_\infty = 0.1$  bar/yr (0.01 MPa/yr) if  $\mu = 30$  GPa. The fit is not significantly different for  $H - a = 10$  or 15 km, with all other parameters the same. Also,  $H$  values from 30 to 40

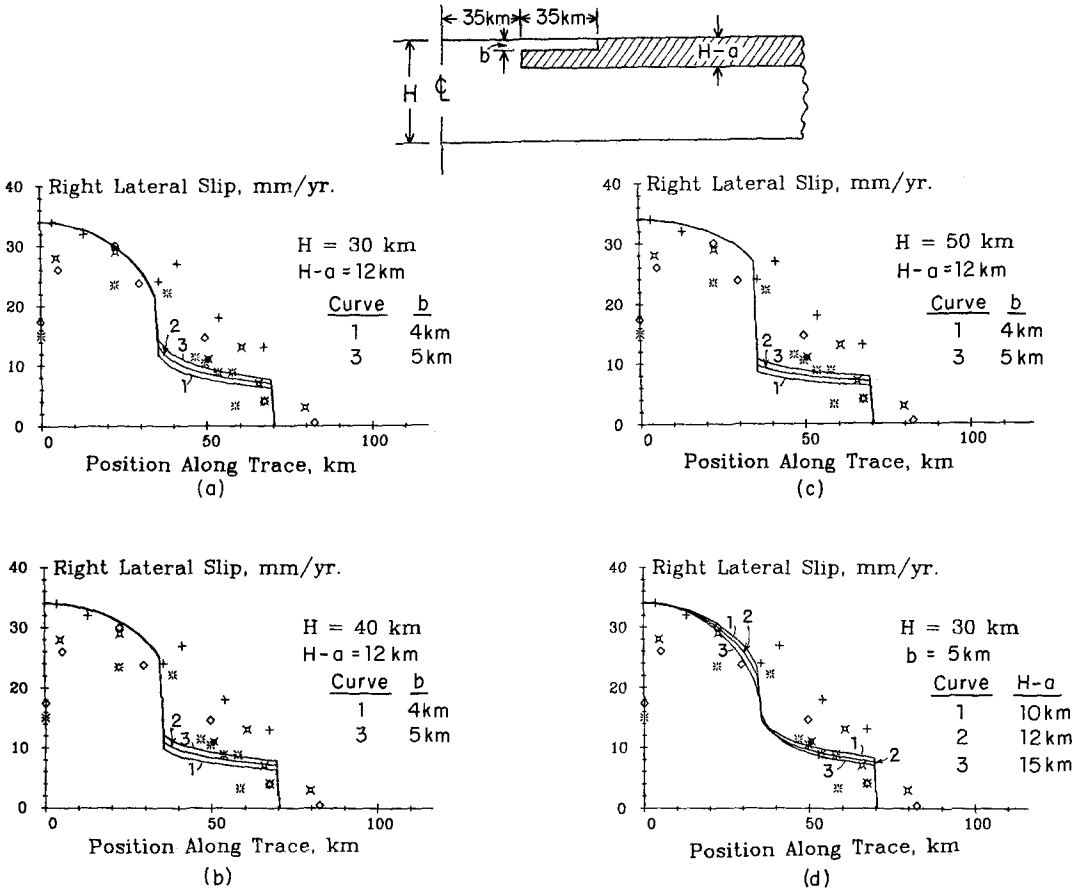


FIG. 11. Effect of variations of model parameters on predicted slip along the fault trace.

km, with other parameters as given in the figure, provide comparably good fits. The most sensitive parameter seems to be  $b$ . Changing  $b$  to 4 km, for example, noticeably alters the fit above the locked patch, again, with other parameters as given. Figure 11 shows results for slip along the fault trace with various choices of parameters for the model with  $H - a_p = H - a_\infty$ .

Let us now consider how the various curves in Figure 10 are calculated. The dashed and dotted curve there is the thickness-averaged slip  $\delta$ , calculated by our modeling procedure, but this cannot be compared directly to measured data. The dashed curve in Figure 10 (and all curves in Figure 11) are slip at the fault trace. We equate this to zero when there is locking to the surface, to  $\delta$  when there is no

locked patch, and to the value calculated in terms of the stress  $\sigma$  by equation (A12) of the antiplane shear analysis when there is a submerged locked patch. It is clear that these last two procedures are accurate well away from transitions in locked zone geometry but not near to such transitions. Indeed, they lead to prediction of a

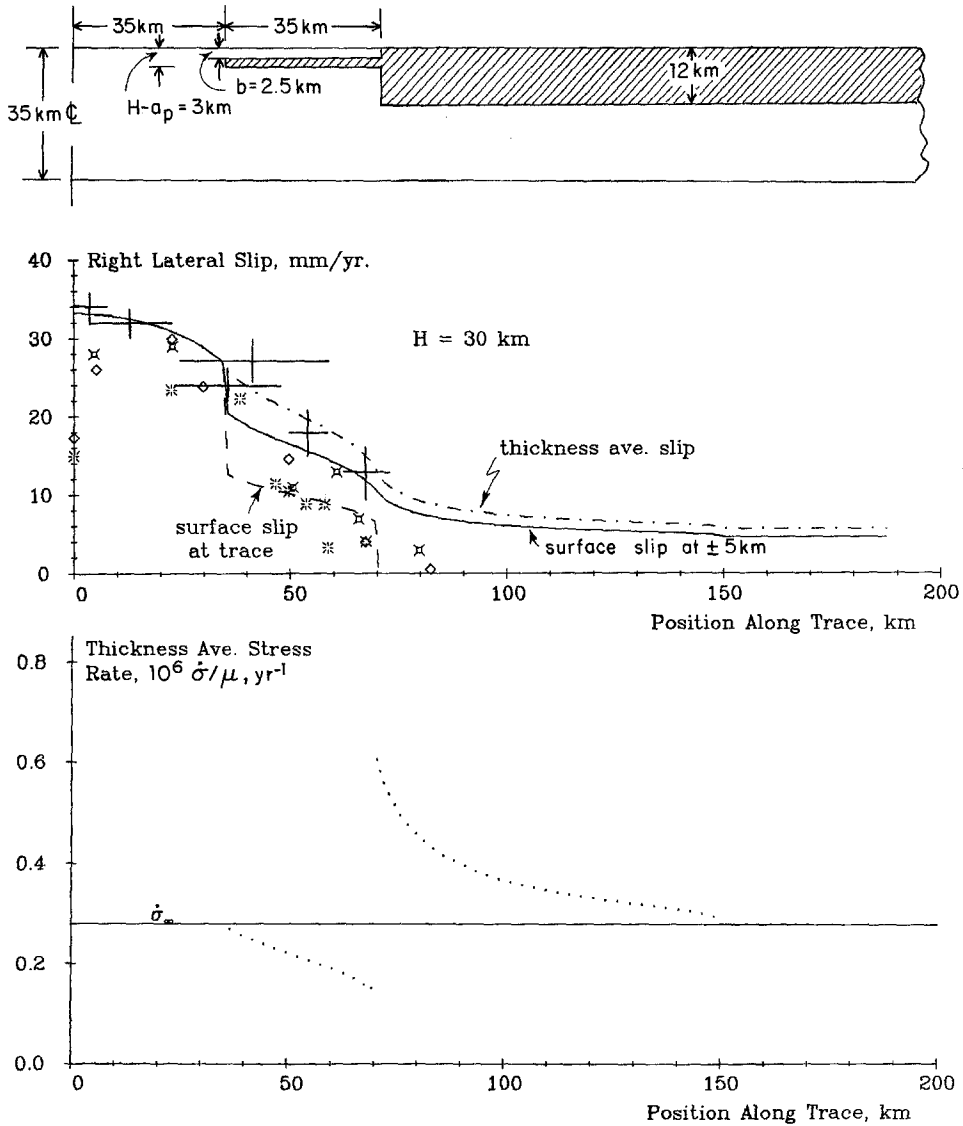


FIG. 12. Better fit to broadscale data provided by locked patch of small area near Parkfield, but location shown is inconsistent with depth of seismicity considerations and nucleation point of 1966 shock, Figure 9.

discontinuous surface slip, as in the figure, at the points of transition in locked zone geometry, whereas the actual surface slip must obviously be continuous. Similarly, the surface slip at  $\pm 5$  km, for comparison with the broadscale measurements, is shown by the solid curve in Figure 10 and is calculated as  $\delta$  when there is no locked patch and from equation (A11) of the antiplane analysis (as twice the value for  $y = 5$  km) when there is a locked patch. This too is inaccurate near transitions.

Thus, the short spatial wavelength inaccuracies inherent to our simple modeling procedure, which are evidently quite pronounced for predictions of surface slip, would seem to mitigate against any further refinement along strike in the locked patch geometry. This is evidently a subject for legitimately three-dimensional stress analysis, as in recent work by Stuart *et al.* (1985) discussed again subsequently. On the other hand, our inferred stressing rate  $\dot{\sigma}_\infty$ , range for lithosphere thickness  $H$ , and stress shed from the creeping section to the 1857 rupture zone are presumably more reliable.

Finally, we show in Figure 12 a fit within the constraints of our segmentation into a 35 km locked strip which more accurately responds to item (1), i.e., to fitting the ratio of broadscale to near-fault slip rate measurements near Parkfield. This gives a locked zone between  $b (= 2.5 \text{ km})$  and  $H - \dot{a}_p$  of only 0.5 km thickness, and the fit of item (1) is seriously degraded by increase of locked zone thickness or by lowering the patch. Thus, this fit seems implausible from the standpoint of item (2), i.e., depth of seismicity. Nevertheless, it is interesting that this very different geometry leads to a similar inferred value for  $\dot{\sigma}_\infty/\mu$  (now  $0.28 \times 10^{-6}/\text{yr}$ ) to that of Figure 10, whereas the stressing rate at the edge of the 1857 rupture zone is now 50 per cent higher.

#### DISCUSSION

One may interpret the fit in Figure 12, demanded by item (1), as suggesting that a small total area of plate boundary is actually locked near Parkfield. Although the geometry of such a small locked zone cannot be constrained accurately by our procedures for the reasons discussed, we suspect on the basis of item (2) that such a patch must extend near Parkfield at least to the nucleation depth around 9 km for the 1966 shock. These requirements argue for a somewhat localized locked patch near Parkfield, and such seems consistent with the work of others. For example, Aki (1979) suggested that the 1966 shock involved rupture of a strong localized barrier, after which the rupture propagated into a region with little strength until arresting at a stopping barrier. [By contrast, Lindh and Boore (1981) seem to argue for a strong locked patch somewhat similar in dimensions but a little shorter than what we showed in Figure 10, terminating at the Gold Hill en-echelon offsets.]

Also, Stuart *et al.* (1985) have recently used three-dimensional elasticity calculations, together with a slip weakening failure model, to simulate near and broadscale slip as measured in the Parkfield area. They obtain reasonable fits to the available geodetic data by a model that has a small slip-deficient patch of approximately 3 km diameter near Parkfield together with a nonslipping rectangular lobe that protrudes 10 km northwestward, between approximately 2 and 8 km depth, from the 12-km-deep locked zone of the great 1857 rupture. They too have problems in reconciling the geodetically constrained model with seismicity and must place their small slip-deficient patch approximately 7 km southeast from, and 2 km shallower than, the 1966 focus. Also, the calculations of Stuart *et al.* (1985), while three-dimensional, are done for an elastic half-space with a rectangular slipping zone (interrupted by locked or slip-deficient regions) extending vertically downwards by 54 km and along strike by 180 km. Their termination of slip at depth and elastic coupling to the remainder of the half-space (compared to our decoupled plate) are presumably the reasons for their inference of a remote stressing rate  $\dot{\sigma}_\infty/\mu = 0.37 \times 10^{-6}/\text{yr}$  which is somewhat higher (by about 30 per cent) than our estimate from Figure 12.

The inference of a small locked area near Parkfield is dictated by the difference

between the broadscale and near-fault slip rate measurements, Figures 7, 10, and 12, as interpreted within a model for which the adjoining plate is ideally elastic. However, there are stress concentrations near the ends of the creeping sections, which are like megascale crack tips, and it is possible that the broadscale measurements have to some extent been affected by nonelastic response in that concentrated stress field. Unfortunately, we do not have knowledge of subsidiary faults in support of this possibility and have no reliable means at present for evaluating how much it could change the conclusions drawn. In calculations which we do not show here, we have also examined the effect of slow upward motion of the lower border of the submerged locked segment in Figures 10 to 12 during the time period of the slip rate measurements. This idea is supported by seismicity migration shown in Figure 9, and it does result in the inference of somewhat larger locked zone areas than in Figure 12, but we were unable to obtain a reasonable fit with the lower boundary of the submerged locked segment remaining below 8 to 10 km, as would seem to be required by Figure 9. Again, this failure to find a suitable fit is to be understood in the context of the 35 km rectangular segment that we use owing to short-wavelength limitations of our model.

On the repeat time scale of order 150 yr for earthquakes such as the great 1857 rupture, Parkfield events might be considered as transients in what averages to steady fault creep. For such time scales, it is appropriate to eliminate the submerged locked patch near Parkfield, and the result is shown in Figure 13 (using  $H - a_\infty = 12$  km). In that figure, we have adjusted the stress rate  $\dot{\sigma}_\infty$  to make the predicted surface slip rate curve agree with measured rates in the middle of the presently creeping section. However, it might be thought somewhat more appropriate to use the same stress rate as inferred in Figure 12, in which case the predicted slip rate curves in Figure 13 should be elevated by about 35 per cent.

The results for slip rate in Figure 13, when compared to the data, also serve to show the need for some sort of locked zone near Parkfield in order to fit the measured slip rates since 1966. We have not been able to resolve the detailed geometry of this zone, but assuming its absence as in Figure 13 results in a significant overprediction of slip rate toward the end of the creeping section of the fault.

The difference between the slip rates of Figure 13 and of Figures 12 or 10, multiplied by a 21 yr Parkfield repeat time, provides an estimate of how much additional slip (short-time preseismic, coseismic, and transient postseismic) is associated with a characteristic Parkfield rupture. The difference in surface slip inferred in this way from Figures 13 and 12 is approximately 0.3 m at the center of the locked patch, whereas Lindh and Boore (1981), citing data from R. D. Brown and J. D. Vedder, infer from offsets of geological and cultural features that total surface slip (including after-slip) reached approximately 0.2 m at points near the center of the fault break. The full predicted difference in slip should be realized only when the asthenosphere has time to relax again to the essentially uncoupled state that we have assumed. This involves a time scale which could possibly overlap with or be longer than the Parkfield repeat time, in which case the differences between Figures 13 and 12 or 10 as discussed cannot be given such a simple interpretation. Subject to the same uncertainties regarding  $\dot{\sigma}_\infty$  and asthenosphere relaxation times, differences between Figures 13 and 12 or 10 in stress rates along the 1857 rupture zone, multiplied by a 21 yr repeat time, also provide a measure of how much additional stress is transferred onto the 1857 zone by a rupture at Parkfield.

The stress rates in Figure 13, when multiplied by a 150 yr repeat time, can be used to estimate the total stress build up between events like the great 1857 rupture. Thus, the accumulated thickness-averaged stress  $\sigma$ , averaged also along strike over the first 10 km southeast from the start of the 12 km deep locked patch that

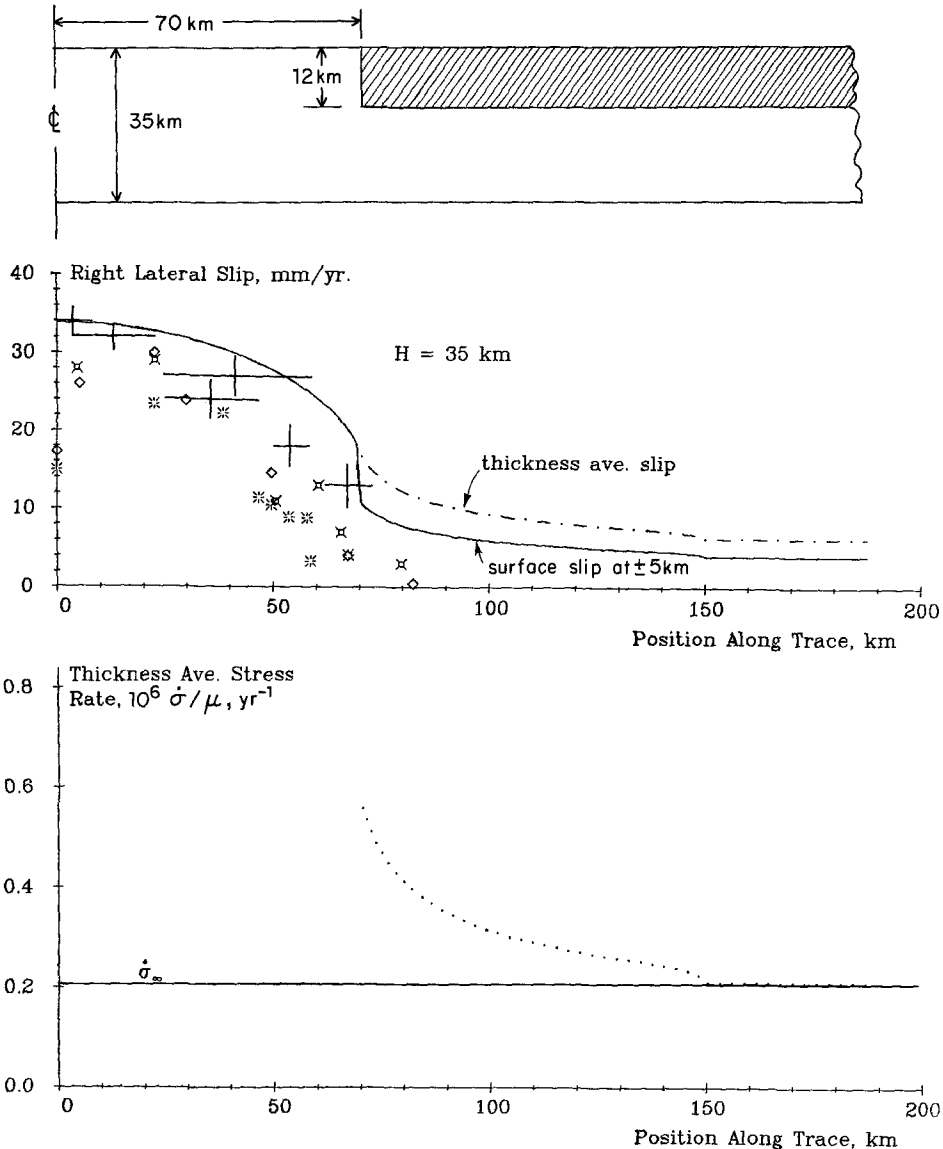


FIG. 13. Model with no locked patch at Parkfield, appropriate for time periods on order of 150 yr on which Parkfield events can be averaged out as steady slip. Note that the overprediction of both near fault and broadscale slip rates since 1966 shows necessity of locked patch near Parkfield.

remains, is found in this way to be approximately 23 bars (2.3 MPa), if  $\mu = 30$  GPa. This amounts to 66 bars ( $23 \times 35/12$ ) if actually averaged over the 12 km locked zone. Using formulas in the Appendix, the stress accumulation results in an accumulated energy release rate  $G$  of about  $1.0 \times 10^7 \text{ J/m}^2$  along the lower margin of the locked patch. This is generally consistent with the representative values of

$4 \times 10^6 \text{ J/m}^2$  to within a factor of 2 or so cited by Li and Rice (1983a) for large plate boundary ruptures, and also with the specific estimate of  $4 \times 10^6 \text{ J/m}^2$  for the 1857 rupture by Rudnicki (1980).

### CONCLUSIONS

In summary, we have demonstrated the use of a simple mechanical model to describe stressing of locked patches along a creeping fault. Stress was seen to be concentrated toward the ends and lower borders of locked zones and to diminish toward their interiors. The high stress concentrations at the ends of the locked zones are interpreted as the cause for the high prerupture seismicity (Dmowska and Li, 1982) in the case of seismic gaps, and for the tendency of a gap-filling rupture to start low in the gap at one end and propagate toward the other.

Using measured slip rates and seismicity patterns along the creeping central portion of the San Andreas fault, we further used the model to infer that there is a submerged transitional locked zone near the Parkfield joining the completely slipping central segment to the northwest and the 1857 rupture zone to the southeast, the latter being currently locked over the seismogenic depth range. Limitations to our modeling procedure prohibit an accurate description of the transition zone geometry, but results suggest that it occupies a relatively small fraction of the area of the normal seismogenic depth range near Parkfield. Our results suggest effective remote stressing rates  $\dot{\sigma}_\infty$  of order  $0.3 \times 10^{-6} \mu/\text{yr}$ , and a less well-constrained lithospheric thickness  $H$  of 30 to 40 km, for consistency with the slip rate data.

Stress accumulation has been inferred for the locked 1857 rupture zone, and an accumulation of fracture energy release capability of order  $10^7 \text{ J/m}^2$  in 150 yr is indicated along the lower margin of that zone, near its northwestern end.

### ACKNOWLEDGMENTS

This work was supported by the NSF and USGS. We are grateful to K. Aki, V. C. Li, G. M. Mavko, K. McNally, W. D. Stuart, W. Thatcher, and R. Wesson for various discussions, and to P. Okubo for comments in review.

### REFERENCES

- Aki, A. (1979). Characterization of barriers on an earthquake fault, *J. Geophys. Res.* **84**, 6140–6148.
- Bakun, W. H. and T. V. McEvilly (1984). Recurrence models and Parkfield, California, earthquakes, *J. Geophys. Res.* **89**, 3051–3058.
- Bakun, W. H., R. M. Stewart, C. G. Bufe, and S. M. Marks (1980). Implication of seismicity for failure of a section of the San Andreas fault, *Bull. Seism. Soc. Am.* **70**, 185–201.
- Burford, R. O. and P. W. Harsh (1980). Slip on the San Andrews fault in central California from alignment array surveys, *Bull. Seism. Soc. Am.* **70**, 1233–1261.
- Delale, F. and F. Erdogan (1982). Application of the line-spring model to a cylindrical shell containing a circumferential or axial part-through crack, *J. Appl. Mech.* **49**, 97–102.
- Dmowska, R. and V. C. Li (1982). A mechanical model of precursory source processes for some large earthquakes, *Geophys. Res. Letters* **9**, 393–396.
- Eaton, J. P., M. E. O'Neill, and J. N. Murdock (1970). Aftershocks of the 1966 Parkfield-Cholame, California, earthquake: a detailed study, *Bull. Seism. Soc. Am.* **60**, 1151–1197.
- Kelleher, J. A. and J. Savino (1975). Distribution of seismicity before large strike slip and thrust-type earthquakes, *J. Geophys. Res.* **80**, 260–271.
- Kelleher, J. A., L. Sykes, and J. Oliver (1973). Possible criteria for predicting earthquake locations and their application to major plate boundaries of the Pacific and the Caribbean, *J. Geophys. Res.* **78**, 2547–2585.
- Kerr, R. A. (1984). Stalking the next Parkfield earthquake, *Science* **223**, 36–38.
- Lay, T. and H. Kanamori (1981). An asperity model of great earthquake sequences, in *Earthquake Prediction: An International Review*, D. W. Simpson and P. G. Richards, Editors, AGU, 579–592.

- Li, V. C. and J. R. Rice (1983a). Preseismic rupture progression and great earthquake instabilities at plate boundaries, *J. Geophys. Res.* **88**, 4231-4246.
- Li, V. C. and J. R. Rice (1983b). Precursory surface deformation in great plate boundary earthquake sequences, *Bull. Seism. Soc. Am.* **73**, 1415-1434.
- Lindh, A. G. and D. M. Boore (1981). Control of rupture by fault geometry during the 1966 Parkfield earthquake, *Bull. Seism. Soc. Am.* **71**, 95-116.
- Lisowski, M. and W. H. Prescott (1981). Short-range distance measurements along the San Andreas fault system in central California, 1975 to 1979, *Bull. Seism. Soc. Am.* **71**, 1607-1624.
- Mavko, G. M. (1984). Large-scale earthquakes from a laboratory friction law (submitted for publication).
- Mogi, K. (1979). Two kinds of seismic gaps, *Pure Appl. Geophys.* **117**, 1172-1186.
- O'Neill, M. E. (1984). Source dimensions and stress drops of small earthquakes near Parkfield, California, *Bull. Seism. Soc. Am.* **74**, 27-40.
- Parks, D. M. (1981). The inelastic line spring: estimate of elastic-plastic fracture mechanics parameters for surface-cracked plates and shells, *Trans. ASME, J. Pressure Vessel Technology* **103**, 246-254.
- Parks, D. M., R. R. Lockett, and J. R. Brockenbrough (1981). Stress intensity factors for surface cracked plates and cylindrical shells using line-spring finite elements, in *Advances in Aerospace Structures and Materials-AD-01*, S. S. Wang and W. J. Renton, Editors, Amer. Soc. Mech. Engr., New York, 279-285.
- Rice, J. R. (1983). Constitutive relations for fault slip and earthquake instabilities, *Pure Appl. Geophys.* **121**, 443-475.
- Rice, J. R. and N. Levy (1972). The part through surface crack in an elastic plate, *J. Appl. Mech.* **39**, 185-194.
- Rudnicki, J. W. (1980). Fracture mechanics applied to the Earth's crust. *Ann. Rev. Earth Planet. Sci.* **8**, 489-525.
- Rymer, M. J., M. Lisowski, and R. O. Burford (1984). Structural explanations for low creep rates on the San Andreas fault near Monarch Park, Central California, *Bull. Seism. Soc. Am.* **74**, 925-931.
- Schulz, S. S., G. M. Mavko, R. O. Burford, and W. D. Stuart (1982). Long-term fault creep observations in central California, *J. Geophys. Res.* **87**, 6977-6982.
- Segall, P. and D. D. Pollard (1980). Mechanics of discontinuous faults, *J. Geophys. Res.* **85**, 4337-4350.
- Stuart, W. D. (1979a). Strain-softening prior to two-dimensional strike slip earthquakes, *J. Geophys. Res.* **84**, 1063-1070.
- Stuart, W. D. (1979b). Strain softening instability model for the San Fernando earthquake, *Science* **204**, 907-910.
- Stuart, W. D. and G. M. Mavko (1979). Earthquake instability on a strike-slip fault, *J. Geophys. Res.* **84**, 2153-2160.
- Stuart, W. D., R. J. Archuleta, and A. G. Lindh (1985). Forecast model for moderate earthquakes near Parkfield, California, *J. Geophys. Res.* **90**, 592-604.
- Tse, S. T. and J. R. Rice (1984). Stick-slip confinement to upper crust by temperature dependent frictional constitutive response (abstract), *EOS, Trans. Am. Geophys. Union* **65**, 993.
- Wesson, R. L., R. O. Burford, and W. L. Ellsworth (1973). Relationship between seismicity, fault creep, and crustal loading along the central San Andreas fault, in *Proceedings, Conference on Tectonic Problems of the San Andreas Fault System*, R. L. Kovach and A. Nur, Editors, *Stanford University Publ. Geol. Sci.* **13**, 303-321.
- Wesson, R. L., R. Robinson, C. G. Bufe, W. L. Ellsworth, J. H. Pfluke, J. A. Steppe, and L. C. Seekins (1977). Search for seismic forerunners to earthquakes in central California, *Tectonophysics* **42**, 111-126.

DIVISION OF APPLIED SCIENCES  
HARVARD UNIVERSITY  
CAMBRIDGE, MASSACHUSETTS 02138

Manuscript received 10 October 1984

#### APPENDIX

Using analytic function theory in two-dimensional linear elasticity, a solution for an unsymmetric double-edge notched plate under antiplane (mode III) loading is derived in this section. As suggested by Figure 2b, the only nonvanishing displace-

ment is  $u(z, y)$  in the  $x$  direction. With the stress-strain and strain-displacement relations, one can rewrite the equilibrium equation as  $\nabla^2 u = 0$  for this case where  $\nabla^2$  is the Laplacian operator in the  $z - y$  plane. Displacement and shear stresses may be then represented in terms of an analytic function  $\omega(z + iy)$  of the complex variable  $z + iy$ ,

$$u = \text{Im}[\omega(z + iy)]/\mu \quad (\text{A1})$$

and

$$\tau_{xy} + i\tau_{xz} = \omega'(z + iy) \quad (\text{A2})$$

where  $\mu$  is the shear modulus.

The aim of this analysis is to find the analytic function meeting appropriate boundary conditions. Since the problem is antisymmetric about  $y = 0$ , we simplify the solution procedure by just considering half of the configuration (i.e.,  $y \geq 0$ ) as shown in Figure A1(a). The stress-free boundary conditions on the crack faces (along  $BD$  and  $AC$ ), and the top and bottom faces of the plate imply  $\partial u/\partial n = 0$  where  $n$  is the measured normal to the faces concerned. The antisymmetry of  $u$  gives  $u = 0$  along  $AB$ . The analytic function may be deduced readily if one first conformally maps the strip in Figure A1(a) into another strip in the  $\xi - \eta$  plane as shown in Figure A1(b) such that the corresponding boundary conditions are

$$\begin{aligned} u &= 0 && \text{along } A'B' \\ \frac{\partial u}{\partial \xi} &= 0 && \text{along } B'D'F_\infty' \text{ and } A'C'E_\infty'. \end{aligned} \quad (\text{A3})$$

It is easily seen that  $u$  is then given by

$$\mu u = A\eta \quad (\text{A4})$$

where  $A$  is to be determined to give the proper thickness averaged stress  $\sigma$  transmitted across the plate boundary. The mapping function for this transformation is

$$\xi + i\eta = \frac{2}{\pi} \sin^{-1} \left\{ \left[ \beta - \alpha - 2 \cos \frac{\pi(z + iy)}{H} \right] / (\alpha + \beta) \right\} \quad (\text{A5})$$

where here and below we use the notations

$$\alpha = \cos(\pi a/H) \quad \beta = \cos(\pi b/H). \quad (\text{A6})$$

[The mapping is generated in steps as follows

$$\Phi + i\Psi = -\cos[\pi(z + iy)/H]$$

maps the strip of Figure A1(a) into the half  $\Psi \geq 0$  of the  $\Phi - \Psi$  plane and

$$2(\Phi + i\Psi) + \beta - \alpha = (\alpha + \beta) \sin[\pi(\xi + i\eta)/2]$$

maps the strip of Figure A1(b) into the same half plane. Elimination of  $\Phi + i\Psi$  gives (A5).]

From equations (A1), (A4), and (A5), the analytic function  $\omega$  is

$$\omega = A(\xi + i\eta) = \frac{2A}{\pi} \sin^{-1} \left\{ \left[ \beta - \alpha - 2 \cos \frac{\pi(z + iy)}{H} \right] / (\alpha + \beta) \right\} \quad (A7)$$

and stresses are calculated from (A2) as

$$\tau_{xy} + i\tau_{xz} = \frac{4A}{H} \sin \frac{\pi(z + iy)}{H} \left\{ (\beta + \alpha)^2 - \left[ \beta - \alpha - 2 \cos \frac{\pi(z + iy)}{H} \right]^2 \right\}^{-1/2} \quad (A8)$$

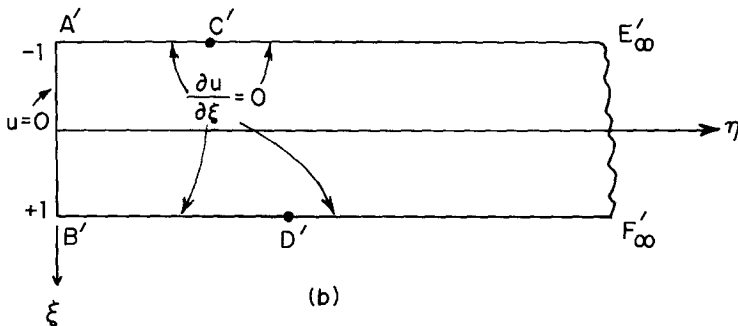
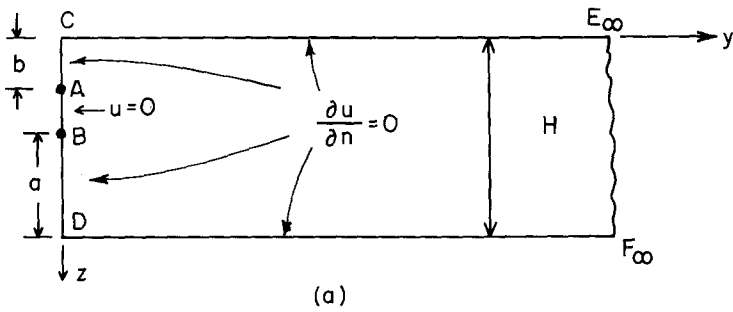


FIG. A1. (a) Half of the cracked strip of Figure 2b, loaded in an antiplane strain. (b) Conformal map of above region to a strip with corresponding points shown.

We may now determine  $A$  by equating the thickness average of  $\tau_{xy}$  to  $\sigma$ . This average is independent of  $y$  and is most readily computed by letting  $y \rightarrow \infty$ , in which case the right-hand side of equation (A8) reduces to  $2A/H$ . Thus,

$$A = \sigma H/2. \quad (A9)$$

Some useful relations can be derived from the foregoing solution. For example, on the Earth's surface ( $z = 0, y \geq 0$ ), the surface shear strain is

$$\frac{\partial u}{\partial y} \Big|_{z=0} = \frac{2\sigma}{\mu} \sinh \left( \frac{\pi y}{H} \right) \left[ \left( 2 \cosh \frac{\pi y}{H} + \alpha - \beta \right)^2 - (\alpha + \beta)^2 \right]^{-1/2} \quad (A10)$$

and the surface displacement itself is given by

$$u \Big|_{z=0} = \frac{\sigma H}{\pi \mu} \cosh^{-1} \left[ \left( 2 \cosh \frac{\pi y}{H} + \alpha - \beta \right) / (\alpha + \beta) \right]. \quad (\text{A11})$$

In particular, the slip displacement discontinuity at the fault trace is

$$\Delta u = 2u \Big|_{z=0, y=0^+} = \frac{2\sigma H}{\pi \mu} \cosh^{-1} [(2 + \alpha - \beta)/(\alpha + \beta)]. \quad (\text{A12})$$

It is easiest to determine the thickness average  $\delta$  of local slip  $\Delta u$  at the plate boundary indirectly by observing that  $\delta$  must appear in a representation of  $u$  in the form

$$u(z, y) = \sigma y/\mu + \delta/2 + S(z, y). \quad (\text{A13})$$

Here the part  $S(z, y)$  is so defined that its average over  $z$  vanishes and  $S(z, y) \rightarrow 0$  as  $y \rightarrow \infty$ . Substituting this representation with  $z = 0$  into (All) and rearranging gives

$$\frac{\cosh \left( \frac{\pi y}{H} + \frac{\pi \mu \delta}{2\sigma H} + \frac{\pi \mu S}{\sigma H} \right)}{\cosh \frac{\pi y}{H}} = \frac{2 \cosh \frac{\pi y}{H} + \alpha - \beta}{(\alpha + \beta) \cosh \frac{\pi y}{H}}.$$

Thus as  $y \rightarrow \infty$  and  $S \rightarrow 0$ , one has

$$e^{\pi \mu \delta / 2\sigma H} = 2/(\alpha + \beta)$$

and therefore

$$\delta = (2\sigma H/\pi \mu) \ln[2/(\alpha + \beta)] \equiv \sigma/k \quad (\text{A14})$$

where  $k$  is the spring constant. The spring constant as so defined is reported as equation (2).

The local shear stress  $\tau_{xy}$  transmitted across the locked portion of plate boundary between  $z = b$  and  $z = H - a$  is

$$\tau_{xy} |_{y=0} = 2\sigma \sin \left( \frac{\pi z}{H} \right) \left\{ (\alpha + \beta)^2 - \left[ 2 \cos \frac{\pi z}{H} + \alpha - \beta \right]^2 \right\}^{-1/2} \quad (\text{A15})$$

for  $b < z < H - a$ . Recalling that the mode III stress intensity factor is defined by

$$K_{III} = \lim_{r \rightarrow 0} \sqrt{2\pi r} \tau_{xy} |_{y=0}$$

where  $r$  is distance into the locked zone ahead of the tip of a slipping crack, one finds

$$K_{III}^{(a)} = \sigma \sqrt{2H \sin(\pi a/H)/(\alpha + \beta)} \quad (\text{A16})$$

for the lower crack tip at  $z = H - a$  and

$$K_{III}^{(b)} = \sigma \sqrt{2H \sin(\pi b/H) / (\alpha + \beta)} \tag{A17}$$

for the upper crack tip at  $z = b$ . If the slipping cracks advance into the locked region by amounts  $\Delta a$ ,  $\Delta b$  the energy (per unit distance along strike)  $G^{(a)}\Delta a$  flows to the lower tip and  $G^{(b)}\Delta b$  to the upper. Here,  $G$  is the energy release rate and is related to  $K_{III}$  by the Irwin formula

$$G = K_{III}^2 / 2\mu. \tag{A18}$$

This last expression was evaluated with the help of equation (A16) and the numerical solution developed for  $\sigma$ , is the source of the fracture energy values inferred in the text.

In fact, the line-spring procedure as outlined in the text implies expressions of

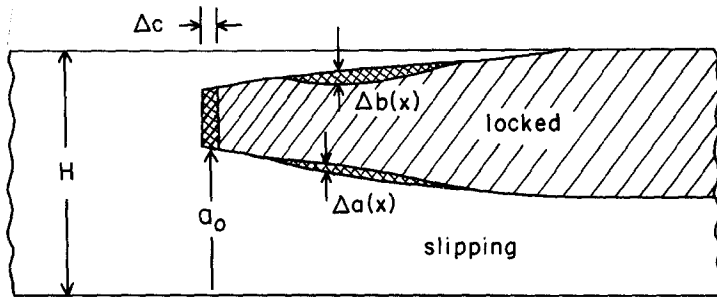


FIG. A2. Explanation of the procedure for calculating crack tip elastic energy release rate for advance of slipping region into the locked patch.

its own for energy release rate. It is interesting to see that these expressions are consistent with what is given above and, also, that they enable the calculation of  $G$  for very general patterns of crack advance. Evidently, the strain energy of the lithosphere expressed consistently with the line-spring procedure is

$$U = H \int_{\text{fault}} \frac{1}{2} \sigma \delta \, dx + H \int_{\text{plate}} \frac{1}{2} \sigma_{\lambda\mu} \epsilon_{\lambda\mu} \, dx \, dy \tag{A19}$$

where  $\lambda$  and  $\mu$  are summed over  $x$  and  $y$ , indexing thickness-averaged stresses and strains in the plate, and where

$$\delta = \sigma/k, \quad \epsilon_{\lambda\mu} = (1 + \nu) \sigma_{\lambda\mu} / E - \nu \delta_{\lambda\mu} (\sigma_{xx} + \sigma_{yy}) / E. \tag{A20}$$

With reference to Figure A2, a pattern of infinitesimal crack advance into the locked region may be described by specifying  $\Delta a(x)$  and  $\Delta b(x)$  and also, when the left border of the locked region is vertical as shown, the advance  $\Delta c$  of this vertical border. Writing the resulting change in  $U$  to first order as products of local  $G$  values times areas swept out, one has

$$\Delta U = -G^{(0)}(H - a^0 - b^0)\Delta c - \int_{\text{fault}} [G^{(a)}\Delta a + G^{(b)}\Delta b] \, dx. \tag{A21}$$

Here "0" refers to values at the left border of the locked region in Figure A2,  $G^{(0)}$  is the average  $G$  from  $b_0$  to  $H - a_0$  along that boundary, and  $G^{(a)}$  and  $G^{(b)}$  are local  $G$  values at the respective lower and upper crack tips.

Now, if  $\Delta k$  denotes the corresponding variation in  $k$  due to  $\Delta a$  and  $\Delta b$  and if  $\Delta\delta$  and  $\Delta\varepsilon_{\lambda\mu}$  denote the variation in the deformation field, necessarily satisfying

$$\int_{\text{fault}} \sigma \Delta\delta \, dx + \int_{\text{plate}} \sigma_{\lambda\mu} \Delta\varepsilon_{\lambda\mu} \, dx \, dy = 0$$

by the principle of virtual work, then direct calculation shows that

$$\Delta U = -\frac{H\sigma_0^2}{2k_0} \Delta c - H \int_{\text{fault}} \frac{1}{2} \Delta(1/k) \sigma^2 \, dx. \quad (\text{A22})$$

Here  $\sigma$  is the thickness averaged stress of the line-spring solution,  $\sigma_0$  is its value at the left boundary, and  $k_0$  is the spring constant (calculated from  $a_0$  and  $b_0$ ) at that same location. Comparing expressions for  $\Delta U$ , one has

$$G^{(a)} = \frac{\sigma^2 H}{2} \frac{\partial(1/k)}{\partial a}, \quad G^{(b)} = \frac{\sigma^2 H}{2} \frac{\partial(1/k)}{\partial b} \quad (\text{A23})$$

and

$$G^{(0)} = \sigma_0^2 H / 2k_0 (H - a_0 - b_0). \quad (\text{A24})$$

When  $k$  is expressed from (A14) or (2), these expressions for  $G^{(a)}$  and  $G^{(b)}$  are found to be identical to those calculated from (A18) through use of (A16) and (A17). In addition, we get an expression for  $G^{(0)}$ .

The latter can be put to good use for approximate calculations. For example,  $G^{(0)}(H - a_0 - b_0)$  may be assumed to be approximately equal to the energy release  $GH$  that would be calculated by standard plane stress crack mechanics if the locked zone in Figure A2 extended through full thickness ( $a_0 = b_0 = 0$ ). In this way, one gets a simple estimate of  $G^{(0)}$  which may be converted via (A24) to an estimate of  $\sigma_0$ . We have found such estimates to compare well with the results of our numerical solutions, e.g., for geometries like those of Figures 4, 10, and 13.

Finally, it is interesting to calculate the ratio  $G^{(0)}/G^{(a)}$  at the left boundary of the locked region in Figure A2. It measures the propensity for mode II crack advance  $\Delta c$  as compared to that for mode III advance  $\Delta a_0$ . The ratio is

$$G^{(0)}/G^{(a)} = (\alpha_0 + \beta_0) \ln[2/(\alpha_0 + \beta_0)] H / \pi (H - a_0 - b_0) \sin(\pi a_0 / H). \quad (\text{A25})$$

For example, when  $b_0 = 0$  as in Figures 4 and 13 and we choose  $H = 30$  km, the ratio is 1.21 for a locked zone depth  $H - a_0$  of 6 km, 0.96 for 8 km, 0.76 for 10 km, 0.61 for 12 km, and 0.44 for 15 km. Thus, locked zones of shallow depth ( $\lesssim 7.5$  km) bordering a freely slipping fault are more severely stressed in mode II from their sides, and deeper zones in mode III from below, assuming that energy available for fracture is the proper measure of severity of stressing.